

Dual-Porosity Hollow Nanoparticles for the Immunoprotection and Delivery of Nonhuman Enzymes

Inanc Ortac,^{*,†,‡} Dmitri Simberg,[#] Ya-san Yeh,[§] Jian Yang,^{||} Bradley Messmer,[‡] William C. Trogler,^{||} Roger Y. Tsien,^{||,⊥} and Sadik Esener^{*,†,‡,¶}

[†]Department of Electrical and Computer Engineering, [‡]UC San Diego Moores Cancer Center, [§]Department of Bioengineering,

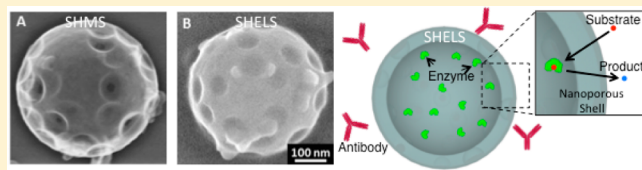
^{||}Department of Chemistry and Biochemistry, [⊥]Howard Hughes Medical Institute and Department of Pharmacology, and

[¶]Department of Nanoengineering, University of California, San Diego, 9500 Gilman Drive, La Jolla, California 92093, United States

[#]University of Colorado, Anschutz Medical Campus, Skaggs School of Pharmacy and Pharmaceutical Sciences, 12850 E. Montview Blvd. V20-4128, Aurora, Colorado 80045, United States

S Supporting Information

ABSTRACT: Although enzymes of nonhuman origin have been studied for a variety of therapeutic and diagnostic applications, their use has been limited by the immune responses generated against them. The described dual-porosity hollow nanoparticle platform obviates immune attack on nonhuman enzymes paving the way to *in vivo* applications including enzyme-prodrug therapies and enzymatic depletion of tumor nutrients. This platform is manufactured with a versatile, scalable, and robust fabrication method. It efficiently encapsulates macromolecular cargos filled through mesopores into a hollow interior, shielding them from antibodies and proteases once the mesopores are sealed with nanoporous material. The nanoporous shell allows small molecule diffusion allowing interaction with the large macromolecular payload in the hollow center. The approach has been validated *in vivo* using L-asparaginase to achieve L-asparagine depletion in the presence of neutralizing antibodies.



KEYWORDS: Nanomedicine, nanoparticles, enzyme encapsulation, nonhuman enzymes, silica, immune response

While enzymes of nonhuman origin are attractive for therapeutic applications, their clinical use has been limited due to the immune response against nonhuman proteins.^{1,2} Different formulations of nonhuman enzymes have shown promise for the treatment of various types of cancer.^{3–6} For example, the treatment of solid or metastatic tumors could benefit from enzyme-prodrug therapies using nonhuman enzymes that convert a noncytotoxic prodrug into its toxic forms at the tumor site by a highly specific localized enzymatic reaction.^{1,7} Another treatment option, which employs nonhuman enzymes, is the depletion of amino acids essential to tumors. This can lead to tumor apoptosis with minimal side effects to normal cells. It is well established that many tumors, including liquid ones, exhibit deficiencies in one or more amino acid synthesis routes, forcing the tumors to rely on an extra-cellular pool of the amino acids for survival and to satisfy protein biosynthesis demands.^{3–5} However, the very ability of nonhuman enzymes to achieve these specific functions causes them to be cleared rapidly or neutralized by the body's immune response, thereby causing failure of these therapies in the clinic.^{8,9}

Therefore, nonhuman enzyme based therapies critically need efficient delivery platforms that can allow stealth operation. This requires preventing antibody and other blood protein access to enzymes, while allowing these enzymes the ability to freely interact with their substrates. Ideally, the delivery

approach must be realized at low cost and complexity without compromising flexibility in design.

Current techniques that aim to prevent immune response created against nonhuman enzymes mainly rely on two general approaches. In the first approach, the enzymes are directly modified with polymers such as polyethylene glycol (PEG)^{10,11} or nanometer scale inorganic/organic networks such as in the case of single enzyme nanoparticles (SENs).^{12,13} Typically with PEG functionalization, which is limited to systemic delivery routes, the activity of the enzymes is reduced significantly although circulation half-life is increased and reduction in immunogenicity is observed compared to the unprotected enzymes.¹⁴ The drawbacks of this approach include antibody generation against PEG, weak retention at the target site, degradation of PEG, and more importantly, the need for extensive optimization of the conjugation chemistry specific for each enzyme type remains a very costly undertaking.¹⁴ SENs also suffer from weak retention at the target site and are applicable only to a limited number of enzymes.¹³

In a second approach that promises lower cost and more generality, enzymes are encapsulated within a protecting structure, which either releases the enzyme at the target^{15–18}

Received: November 24, 2013

Revised: January 17, 2014

Published: January 28, 2014

or allows substrate to access the enzyme.^{19–23} The approaches that depend on release of the enzymes often suffer from nonspecific release as well as inefficient synthesis and loading.^{15–18} Indeed, the encapsulation of enzymes in nano- and mesoporous matrices made of materials such as silica,^{20,24} polyelectrolyte,²² or polymer¹⁹ and inorganic hollow nanoparticles such as gold²³ have been widely studied. However, these approaches also suffer from limitations, which include low loading efficiencies, reduced activity of the enzymes as a result of immobilization and encapsulation chemistries, stability, toxicity, and applicability issues.^{20–23} In addition, these approaches can only be applied to a small number of enzymes due to harsh chemistries involved in the loading process.^{20,23} Furthermore, most of these applications are limited to a narrow range of sizes and materials.^{15–17,20–24} To succeed in the therapy of multidimensional diseases, such as cancer, a generalized nanocarrier platform needs to address all these requirements simultaneously.

In this paper, a robust manufacturing approach is introduced for a versatile class of nanoparticles that can lead to a universal *in vivo* delivery platform for nonhuman enzymes. The platform exhibits key necessary features including exquisite control in synthesis; high enzyme entrapment capacity; efficient protection from neutralization, antibody access, and proteolysis; unperturbed *in vivo* enzyme activity; and long *in-tissue-residence* and stability. We describe the fabrication of dual-porosity hollow nanoparticles called synthetic hollow mesoporous nanospheres (SHMS), which consist of nanoporous (pore size <2 nm)²⁵ material and at the same time have a mesoporous (pore size, 5–50 nm)²⁵ shell (Figure 1A). The nanoporous shell is suitable for diffusion of small molecules while preventing large molecule trafficking. On the other hand,

the larger mesopores on these SHMS can be designed large enough to enable the hollow core of the nanoparticle to be efficiently loaded with large molecules (Figure 1A). Once loaded, the mesopores are sealed with the same nanoporous material, thus forming synthetic hollow enzyme loaded nanospheres (SHELS) encapsulating the large molecule payload. SHELS behave like nano tea bags selectively enabling the payload to interact freely and effectively with smaller molecules in the environment through their nanoporous shells while preventing the escape of the large molecule payload (Figure 1B).

Although SHELS can be manufactured with a variety of materials, we show here that SHELS can be produced from silica with a high yield and scalable synthesis method that utilizes a templating reaction on unmasked parts of the shell surface. Nanomasking is used for the formation of mesopores in the a few nanometers to 50 nm size range with precise control in the masked regions of silica SHMS. We show that once sealed silica SHELS effectively encapsulate enzymes while smaller substrates easily reach, interact with, and are modified by the encapsulated enzymes within the hollow core and diffuse out (Figure 1C). We specifically show that silica SHELS protect immunogenic enzymes from antibody access, neutralization, and proteolysis without loss of functionality in serum immunized against the load for at least two weeks. The experiments demonstrate *in vivo* localized activity in addition to *in-tissue-residence* time of about two months when SHELS are injected intramuscularly. Because SHELS are thin hollow nanospheres, little inorganic mass is introduced minimizing toxicity risks while maximizing load entrapment capacity.

Nanomasking Process and Fabrication of Synthetic Hollow Mesoporous Nanospheres (SHMS). The use of colloidal particles with hollow interiors has been considered promising for the controlled release of drugs and biological molecules, for immune isolation and protection of biomolecules and of biologically active species, and for waste removal^{26–33} due to their high surface area and hollow interior for loading and templating.^{26,27,34} The fabrication of porous hollow particles is commonly reported using template-based synthesis approaches with materials such as vesicular solution, colloids, emulsion droplets, and polymers as templates for forming a layer of target material or its precursor. The core material is subsequently removed by methods such as calcination and dissolution to generate the hollow shell.^{35–37} However, a flexible fabrication approach that allows for the synthesis of hollow particles with a broad range of precise size and specific dual porosity has yet to be developed.

With the existing methods, porosity is primarily defined by the shell material resulting in pores of up to a few nanometers in size.^{38–40} This results in relatively low permeability, preventing the diffusion of macromolecules such as enzymes, proteins, or larger biologically active materials.³⁰ Other approaches exist to create mesoporous particles reaching porosities of several tens of nanometers; however these techniques lack precise control of the pore size and are not applicable to nanopore diameters. These methods also have constraints in the overall particle dimensions.^{30,33} Such approaches typically use a specific property of a given material to create porosity and do not provide a generalized method that can be applied to a large selection of materials. Therefore, a generalized fabrication technique for synthesizing porous particles with any desired specific dimensions, materials and

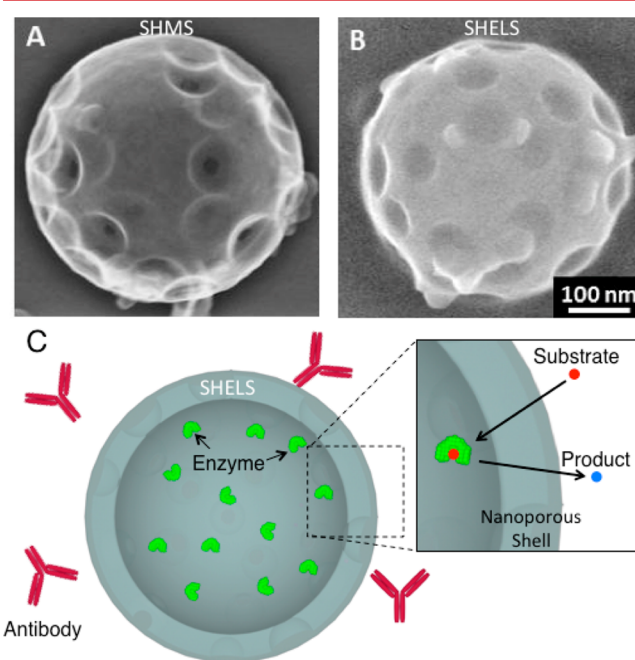


Figure 1. Scanning electron micrographs of (A) Synthetic hollow mesoporous nanospheres (SHMS) and (B) SHELS. Scale bar refers to both (A) and (B). (C) Enzymes encapsulated within the hollow core of SHELS cannot escape. As depicted in the inset, showing the blow-up of a section of SHELS, the small molecule substrate (red dots) can diffuse through the nanoporous shell, interact with the enzyme and diffuse out of SHELS modified (blue dots).

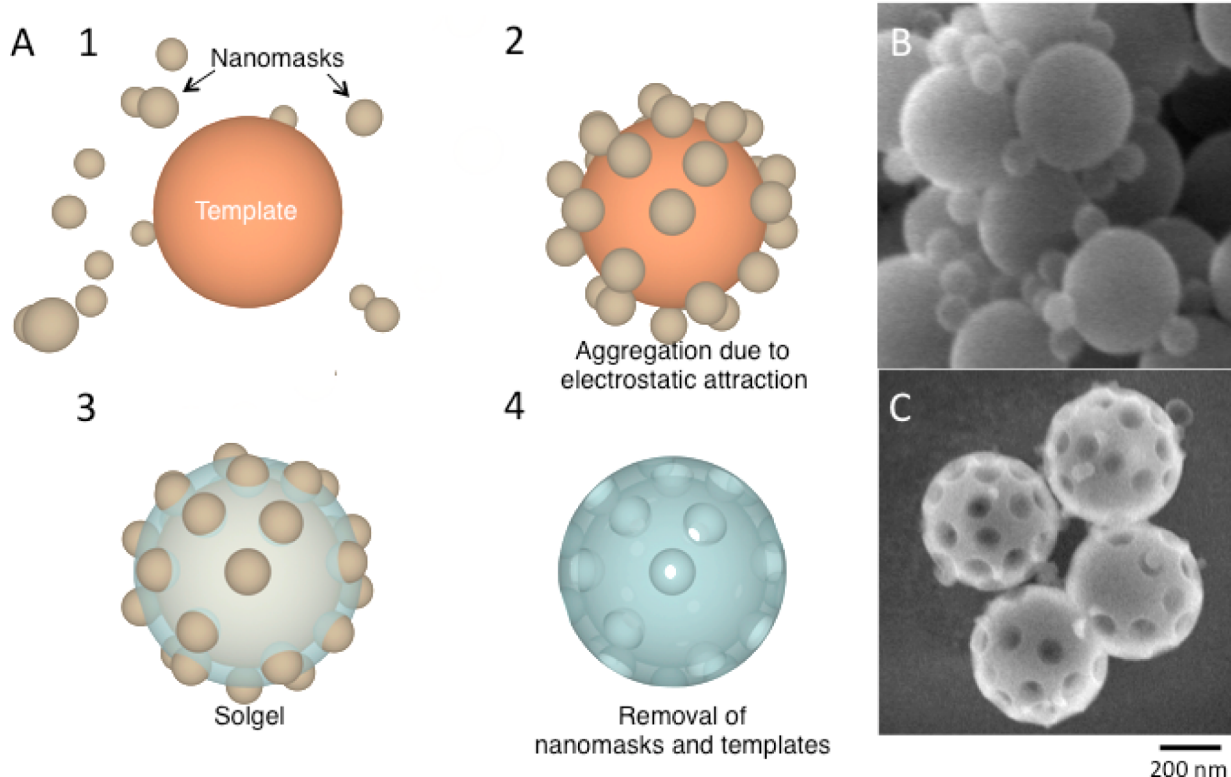


Figure 2. Nanomasking method (A) 1. Amine-functionalized polystyrene nanoparticles (templates) and carboxy-functionalized polystyrene nanoparticles (nanomasks) are mixed in solution. 2. Templates and nanomasks attract each other resulting in aggregation. 3. Followed by addition of sol–gel reactants, the silica polycondensation reaction occurs on the basic template surface while nanomasks block the reaction at the point of contact with the templates. 4. Polymer templates and nanomasks are removed by calcination or dissolution to generate SHMS structure. (B) Scanning electron micrograph of aggregated templates and nanomasks. (C) Scanning electron micrograph of silica SHMS. Scale bar refers to both (B) and (C).

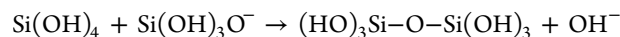
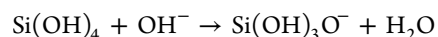
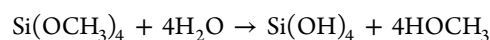
porosity is needed to further expand the potential applications of these particles.

Nanomasking is a template-based approach that can potentially use a variety of materials to prepare hollow particles with monodisperse sizes ranging from 10 to 20 nm to micrometers and with surface pores of controllable sizes from a few nanometers to tens of nanometers. With nanomasking method, SHMS can be manufactured with a precise control in size and permeability in a wide range of scales with various materials. In this approach, blocking materials prevent the growth reaction on parts of the surface and concomitantly create mesopore features on the surface. This technique provides independent control of the particle permeability and size. The overall size of the particle is determined by the template particle. The diameter of the pores can be adjusted by varying the size of the masking particle, and the number of mesopores on the particle surface is controlled by the relative molar concentration of template and masking particles.

Silica was selected as a suitable and practical material to demonstrate SHMS and SHELS because of its biodegradability, biocompatibility and low toxicity thus making it suitable for *in vivo* applications.^{38,41–43} In addition, silica has adjustable porosity, thermal and mechanical stability, low density, and high specific surface area.^{15,16,44,45}

For silica SHMS, amine-functionalized polystyrene nanoparticles are used as templates for nucleating growth of the nanoporous silica solgel network.³⁷ Tetramethoxysilane (TMOS) is hydrolyzed in aqueous solution to give silicic acid, which acts as a precursor for the polycondensation

reaction on the particle's surface. The initial chemistry of the process is shown below³⁷



The synthesis approach is demonstrated in Figure 2. In order to generate the SHMS structure, carboxy-functionalized polystyrene latex nanoparticles as nanomasks are first mixed with larger templates (Figure 2A.1). Particles with oppositely charged surface functional groups attract each other in solution, causing aggregation (Figure 2A.2).

Figure 2B shows a scanning electron micrograph (SEM) micrograph of the framework for SHMS synthesis made up of 500 nm templates and 100 nm nanomasks. The basic nature of the amine-functionalized surface creates a more efficient nucleation site for base-catalyzed silica gel growth compared to the acidic carboxy functionalized surface. At the point of contact, they serve as negatively charged nanomasks for the sol–gel reaction on the particle surface (Figure 2A.3).

Once the silica layer is formed with the desired thickness, the polystyrene particles are removed by dissolution or calcination leaving the silica SHMS structure (Figure 2A.4). Resultant SHMS are shown in the SEM micrograph in Figure 2C. Later, the SHMS are resuspended and dispersed in water using vortex mixing and gentle sonication. The final particle diameter after calcination is about 85% of the diameter of the initial 500 nm

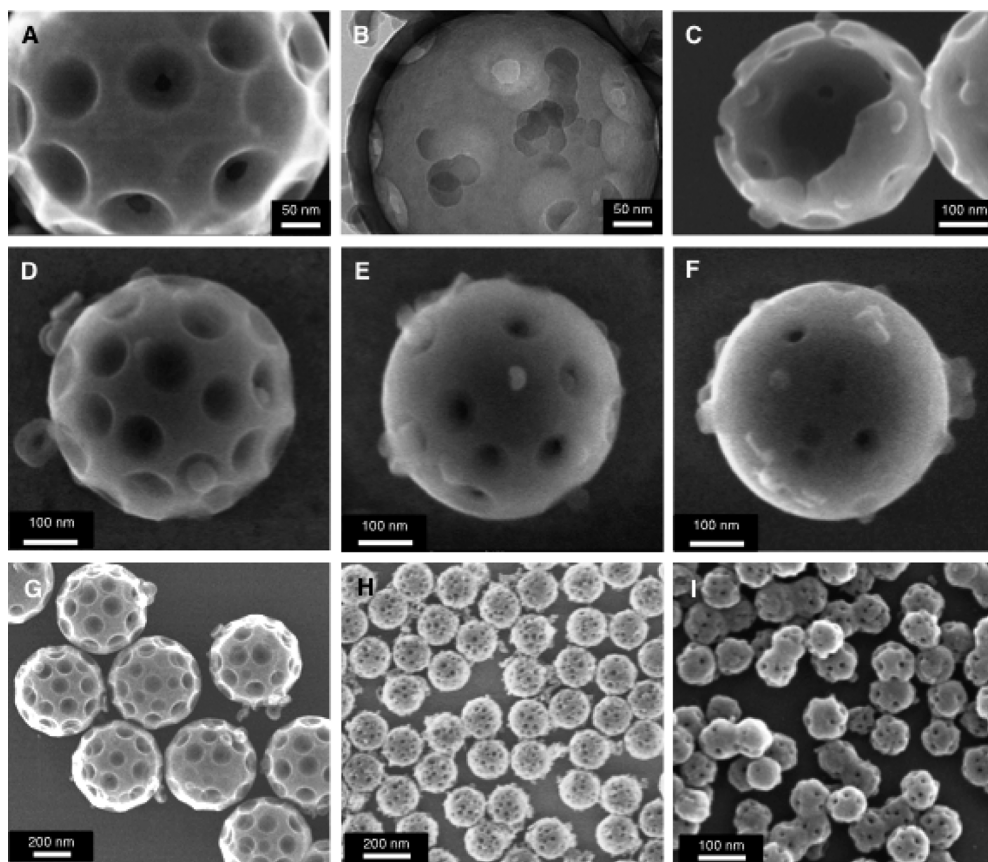


Figure 3. (A–E) Electron micrographs of silica synthetic hollow mesoporous nanospheres (SHMS) made from 500 nm templates and 100 nm. (A) Electron micrograph revealing the surface topography of SHMS taken with secondary electron mode of scanning transmission electron microscope (STEM). (B) Transmission electron micrograph of a SHMS. (C) Scanning electron microscope (SEM) image of a cracked SHMS showing the holes from the interior perspective. (D) SHMS made by 500 nm templates and 100 nm nanomasks with the particle number ratio of 1:30 and (E) 1:15. SHMS made by (F) 500 nm templates and 60 nm nanomasks, (G) 200 nm templates and 40 nm nanomasks, (I) 100 nm templates and 20 nm nanomasks.

template nanoparticles, which may be related to partial dehydration of the silica gel hydroxyl groups during heating or extraction with anhydrous solvents.⁴⁴

The structural properties of SHMS are shown in Figure 3. Higher-resolution electron micrographs taken using the secondary electron mode of a scanning transmission electron microscope (STEM) and a transmission electron microscope (TEM) are presented in Figure 3A,B, respectively, revealing the structure of the generated holes. Silica formation is blocked around the point of contact between two particles, and the curvature of the nanomask surface is reflected by the surface topography of the resultant particle (Figure 3A). The synthesis using 500 nm templates with a TMOS-to-template-weight ratio of 3:1 results in silica shells with a thickness of ~25 nm. This thickness seems to yield stable particles in this size range. The open-hole structure throughout the shell and the thickness of the shell are illustrated by the scanning electron micrograph of a cracked SHMS from the interior perspective in Figure 3C.

This fabrication procedure can be applied to particles with different features in a wide range of sizes from 10 to 20 nm to several micrometers. There are three main degrees of freedom in the fabrication of SHMS: the number of mesopores on the surface (Figure 3D,E), diameter of the mesopores (Figure 3F), and overall particle size (Figure 3G–I). The average number of mesopores on the surface is controlled by the relative molar concentration of templates and nanomasks. SEM micrographs

in Figure 3E,F show the mesopore distribution on the surface when the template-to-nanomask molar ratios in solution are 1:30 and 1:15, respectively. These ratios result in 25–30 holes per particle for the 1:30 ratio (Figure 3E) and 10–15 holes per particle for the 1:15 ratio (Figure 3F). The size of the holes created on the surface can be adjusted by selecting nanomasks with different diameters independently of the overall diameter of the SHMS. Figure 3E,F shows mesopores created using nanomasks with diameters of 100 nm, and Figure 3G shows particles created using nanomasks with 60 nm diameters, all on 500 nm templates. The use of 100 nm nanomasks produces mesopores of 30 ± 4 nm in diameter, and the use of 60 nm nanomasks produces mesopores of 20 ± 3 nm in diameter at the point of contact. Nanomasks down to 20 nm in diameter are available commercially, theoretically yielding mesopores down to several nanometers with high accuracy. The overall size of the SHMS depends on the template particle size, and templates can be obtained in a wide range of sizes. Figure 3G shows particles made with 500 templates and 100 nm nanomasks. Figure 3H shows particles made with 200 nm templates and 40 nm nanomasks. Figure 3I shows particles made with 100 nm templates and 20 nm nanomasks.

All template and nanomask particle combinations resulted in mesopores about 25–35% of the diameter of the initial nanomasks, decreasing slightly with smaller dimensions. The slight decrease for smaller nanomasks might be related to the

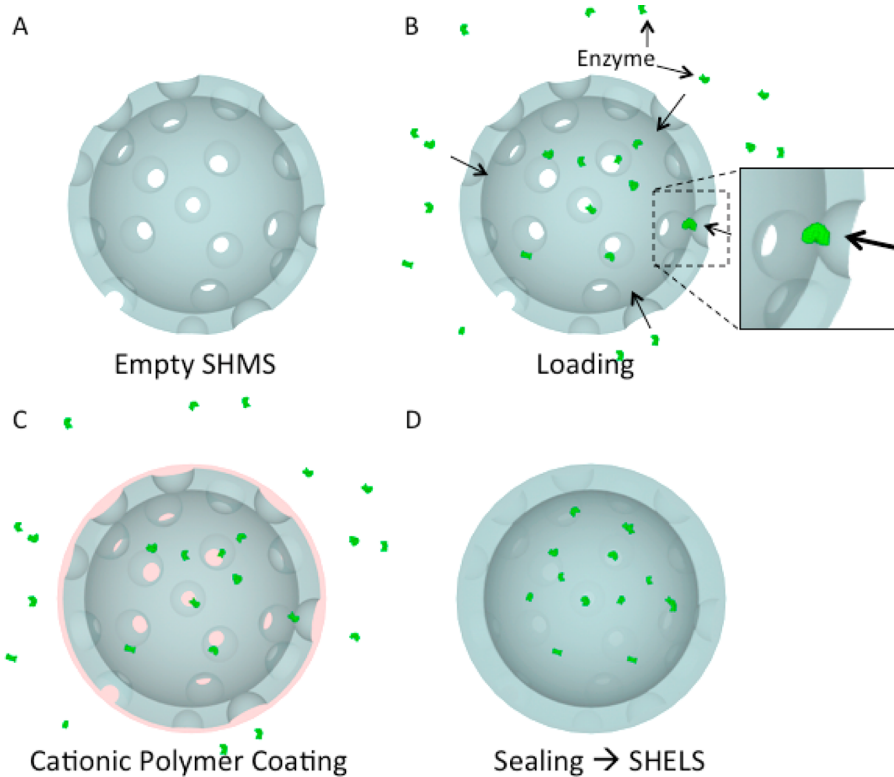


Figure 4. The sealing concept and SHELS. Illustrations show the cross sections. (A) Empty SHMS. (B) High concentration of enzyme is added to the SHMS suspension and diffuses into the hollow interior of SHMS. The inset shows a blowup of a part of SHMS, depicting an enzyme diffusing through a mesopore. (C) Interior enzyme concentration is equilibrated with exterior. Poly-L-lysine is added to convert the surface charge. (D) SHMS are coated with another layer of porous material sealing enzymes within the particle.

particles' increasing surface curvature, resulting in a smaller point of contact. The diameter of the mesopores formed on the SHMS fabricated using the 200 nm template/40 nm nanomask pair is 12 ± 2 nm (Figure 3H), whereas the diameter of the mesopores formed on the SHMS fabricated using the 100 nm template/20 nm nanomask pair is 5 ± 3 nm (Figure 3I). Removal of the core by calcination results in an isotropic shrinking of hydrated SHMS. The fabrication approach results in monodisperse and uniform particles for all three sizes, as shown in the electron micrographs in Figure 3G–I; the particles' monodispersity in suspension was validated by dynamic light scattering (see Supporting Information, Figure S1). Dynamic light scattering measurements yield average hydrodynamic radii of 110 ± 5 , 221 ± 8 , and 534 ± 13 nm for particles made with 100, 200, and 500 nm templates, respectively. Their polydispersity indexes end up 0.120 ± 0.011 , 0.134 ± 0.013 , 0.111 ± 0.022 , respectively.

Loading, Sealing, and Formation of SHELS. SHMS are loaded by diffusion of macromolecules through their mesopores (Figure 4A). As the mesopores are relatively large (typically >5 nm) compared to many enzymes, enzymes can diffuse freely and quickly into the structure to equilibrate the concentration inside and outside of SHMS (Figure 4B). Later, a new layer of nanoporous material is formed around the particle surface, closing the mesopores within the nanoporous surface (Figure 4C). In the case of silica, the SHMS surface is negatively charged due to SiO^- groups. A positively charged polymer such as poly-L-lysine is added to adsorb to the surface of the particles and change the surface charge to positive. TMOS is then added to grow new silica on the surface and close the mesopores of SHMS, converting them to SHELS. This reaction occurs in

near-neutral buffer conditions and does not damage the enzyme. Once the mesopores are closed, the load is encapsulated within SHELS and cannot escape (Figure 4D). However, the load can still interact with small molecules in the surrounding environment via diffusion through nanopores.

This capability provides two unique benefits, as discussed in the next section. First, the enzyme is essentially hidden from the immune system because antibodies are too large to pass through the nanopores. Therefore, the enzyme is protected from the immune system and from digesting enzymes, such as proteases, while remaining completely active. Second, SHELS can be coated with passivating and targeting ligands without any chemical modification of the payload, making them a simple yet effective vehicle for in vivo applications.

Characterization of SHELS Loading, Enzymatic Activity and Protection Abilities. Penicillinase from *Bacillus cereus* is a member of the family of beta-lactamases that catalyze the hydrolysis of the beta-lactam ring.⁴⁶ *B. cereus* penicillinase was selected for the characterization of SHELS because it is the preferred beta-lactamase for enzyme-prodrug based therapies,^{6,7,47} and sensitive chromogenic and fluorogenic assays are available.⁴⁸ The latter used the substrate CCF2, which contains a coumarin linked to fluorescein via a cephalosporin group. Before cleavage by penicillinase, excitation of the coumarin at 409 nm causes efficient fluorescence resonance energy transfer (FRET) to fluorescein, resulting in green emission peaking around 520 nm. Penicillinase cleaves the cephalosporin group, separating fluorescein from coumarin and disrupting FRET, so that the same excitation produces blue 447 nm emission from coumarin. CCF2 is sold commercially as an acetoxyethyl (AM) ester, which rapidly reverts to CCF2 on

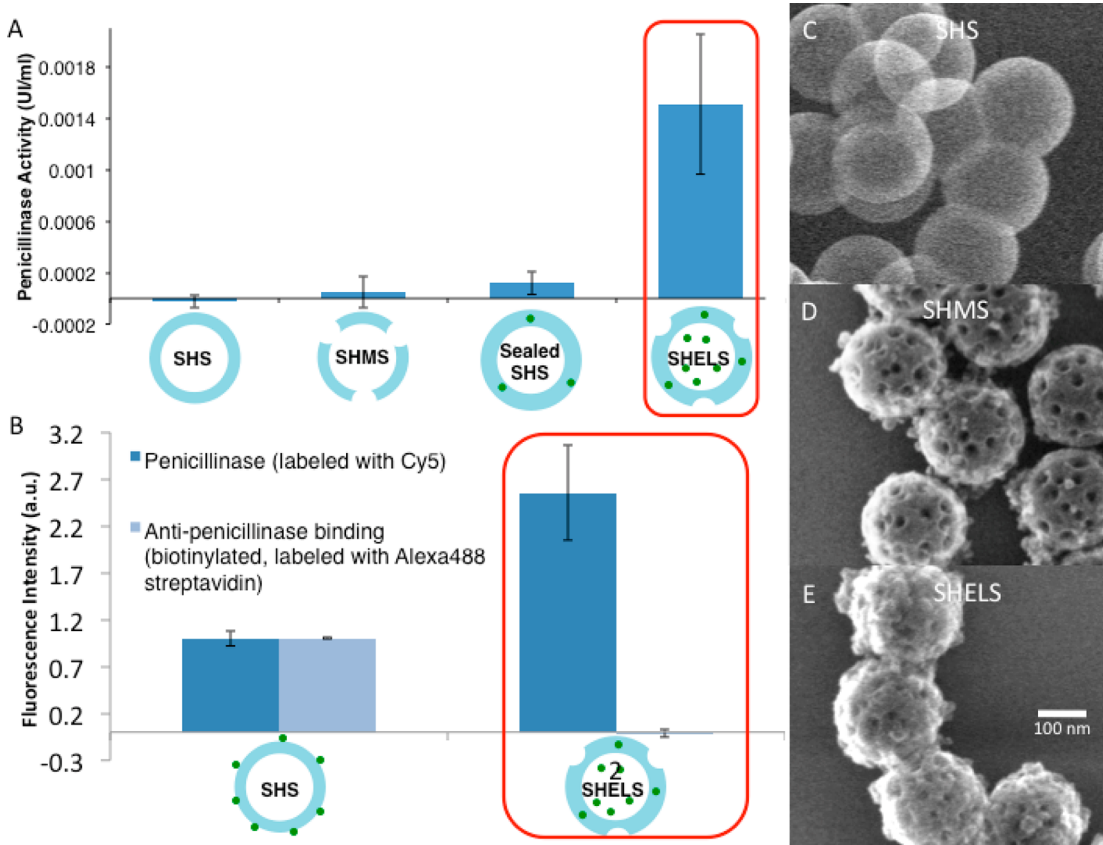


Figure 5. (A) Activity comparison for SHELS with encapsulated penicillinase and CCF2-AM as substrate in normal serum. From the left: first group, hollow silica nanospheres (SHS); second group, SHMS; third group, sealed SHS; fourth group, SHELS. (B) Polyclonal antibody binding against encapsulated penicillinase. Dark blue bars represent the fluorescence from Alexa 488 with streptavidin that can attach antibody molecules with biotin. Light blue bars represent fluorescence from Cy5 labeled penicillinase. (Left) Penicillinase adsorbed on the surface of hollow silica nanospheres. (Right) Penicillinase encapsulated within silica SHELS, which was incubated with proteinase-K followed by successive washing before measurement. (C) Two hundred nanometer hollow silica nanospheres. (D) SHMS made with 200 templates and 40 nm. (E) SHELS made by sealing SHMS similar to (D). Error bar refers to panels C–E. Error bars correspond to standard deviation of at least three replicate experiments.

exposure to esterases in rodent plasma and serum, as well as inside cells.^{48,49}

Figure 5.A shows activity of penicillinase (MW = 28 kDa) enzyme encapsulated within SHELS. All samples were exposed to proteinase-K, which digests proteins (see Supporting Information, Figure S2); therefore, sustained activity of the encapsulated enzyme after exposure to proteinase-K demonstrates protection of the enzyme against proteolysis by encapsulation in SHELS.

In Figure 5.A, the left-most bar represents silica synthetic hollow nanospheres (SHS) fabricated by sol–gel templation over 200-nm templates without mesopores on the surface.³⁷ Therefore, enzymes can only be adsorbed on the surface (Figure 5.C). The second bar from the left represents SHMS made with 200-nm templates and 40-nm nanomasks (Figure 5.D). Both SHS and SHMS were incubated with 26.4 μ M *B. cereus* penicillinase solution. The third and fourth bars from the left (Figure 5.E) represent particles similar to SHS and SHMS, respectively, except that the sealing reaction was performed after enzyme incubation, thereby encapsulating enzymes within the structure. Later, all four groups were washed successively, removing unbound and free enzymes, and subsequently incubated with proteinase-K to remove the enzyme molecules stuck on the surface.

SHS and SHMS exhibit no or very little activity (Figure 5.A), which is expected after exposure to proteinase-K. Sealed SHS

show about a 2-fold increase in activity over SHS; this is brought about by the protection provided by the second layer of silica over the enzymes stuck on the surface and thereby supporting the protective effect of the additional sealing silica layer. However, there is a significant increase in activity in SHELS (outlined in red). The 10-fold activity increase of SHELS over sealed SHS indicates that the increase is not due to the enzyme covering the surface but rather is caused by the enzyme molecules filling the hollow interior. This dramatic difference between SHMS and SHELS clearly establishes the superiority of using SHELS, as both samples have gone through the same process except for the additional sealing step on SHELS.

With the current protocol, comparing with the standard curve of free *B. cereus* penicillinase (see Supporting Information, Figure S3), the measured activity corresponds to 6×10^{-14} international units (IU) from a single 200 nm SHELS corresponding to ~67 enzyme molecules per particle (see Supporting Information, Figure S4). During enzyme loading, SHMS were initially incubated with 26.4 μ M enzyme solution. The assayed concentration of enzyme within a single SHELS corresponds to ~26 μ M, resulting in a 98–100% match with the exterior loading concentration. This result also shows that there is no measurable loss of activity of enzyme during the loading and sealing process or by hindered diffusion of substrate through the nanoporous shell in this interior

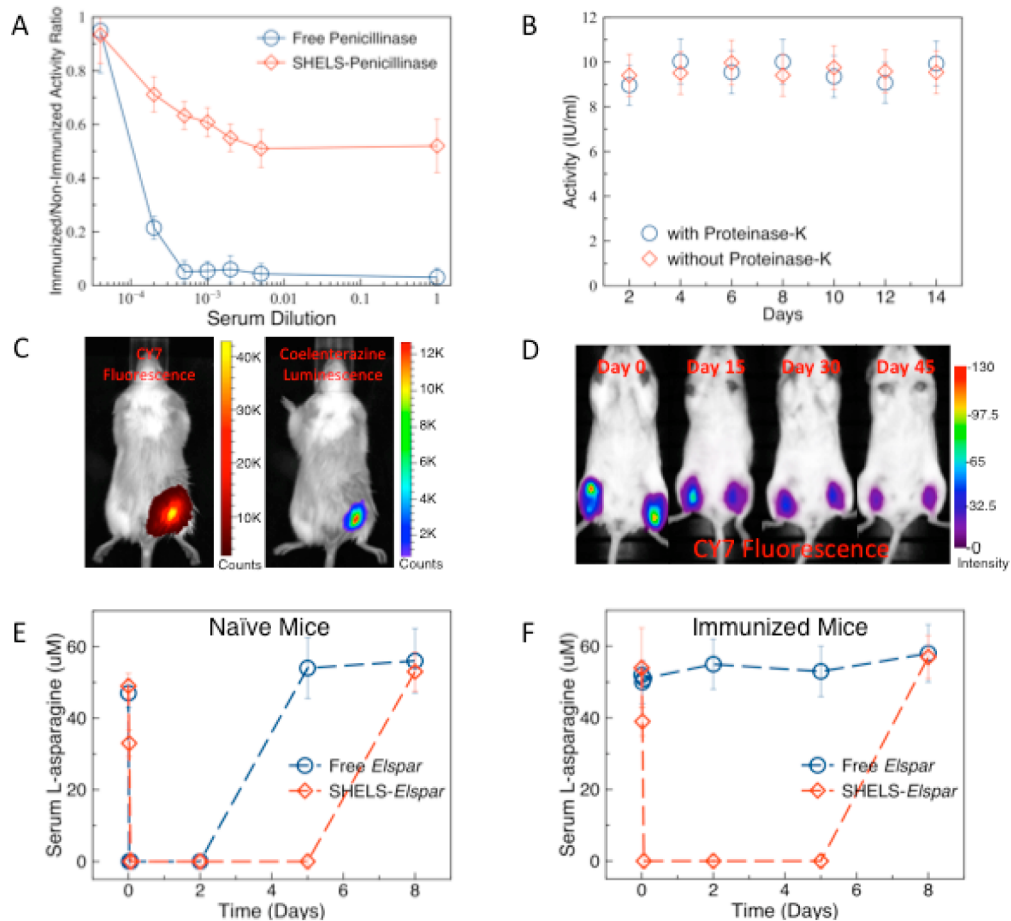


Figure 6. (A) Neutralization test in the presence of antibodies. The ratios of activity on nitrocefin ($50 \mu\text{g}/\text{mL}$) in serums post- to preimmunization are used as the vertical axis. Circles, free penicillinase; diamonds, penicillinase encapsulated SHELS with bare silica surface. (B) Sustained activity of penicillinase loaded SHELS for 15 days with the presence (triangles) and without the presence (squares) of proteinase-K in serum from mice immunized with penicillinase previously. (C) Demonstration of in vivo activity of *Gaussia princeps* luciferase encapsulated in SHELS labeled with Cyanine 7 (Cy7) dye. Fifty microliters of *Gaussia princeps* luciferase (GaLuc) enzyme encapsulated SHELS solution with a concentration of $\sim 4 \times 10^{12}$ particles/ml was injected subcutaneously into BALB/c mice, followed by lateral tail vein injection of $150 \mu\text{g}$ native-coelenterazine after 5 min. (Left) Cy7 fluorescence overlaid with illuminated image. (Right) Native-coelenterazine luminescence overlaid with illuminated image. (D) Localization of intramuscularly injected penicillinase loaded SHELS labeled with Cy7 at days 0, 15, 30, and 45. Error bars correspond to standard deviation of at least three replicate experiments. (E) In vivo L-asparagine depletion in naïve mice. Free Elspar (circles) and SHELS-Elspair (diamonds) were injected intramuscularly into naïve mice with equivalent units of activity. Serum L-asparagine level pre and post injection up to 8 days was measured. (F) In vivo L-asparagine depletion in passively immunized mice. Free Elspar (circles) and SHELS-Elspair (diamonds) were injected intramuscularly to passively immunized mice with equivalent units of activity. Serum L-asparagine level pre and post injection up to 8 days was measured. Error bars correspond to standard deviation of at least three replicate experiments.

concentration of enzyme. With this procedure, we have shown that it is feasible to achieve $>1500 \text{ mg/g}$ enzyme entrapment capacity in silica SHELS using *B. cereus* penicillinase (MW 28 KDa) (see Supporting Information, Figures S5 and S6). The evaluation of entrapment capacity for different enzymes with varying molecular weights needs further investigation.

Figure 5.B evaluates antibody access to the enzyme encapsulated in SHELS. For this demonstration, the penicillinase was fluorescently labeled with Cy5, and its accessibility was probed with a rabbit polyclonal biotinylated antibody against penicillinase, detected by Alexa488 labeled streptavidin. The dark blue bar on the left-hand side depicts fluorescence from enzyme molecules adsorbed on the surface of SHS, while the dark blue bar on the right-hand side depicts fluorescence from penicillinase enzymes encapsulated within SHELS. Both sets were incubated with proteinase-K to remove any enzyme that might have been stuck on the surface and were washed several times to remove unbound enzymes. The light

blue bars are Alexa488 fluorescence intensities that represent antibody binding. In the case of surface-adsorbed penicillinase, significant antibody binding is observed. However, when penicillinase is encapsulated within SHELS, no such antibody binding is observed. Although the amount of encapsulated penicillinase within SHELS is about 2.5 times more than surface-absorbed penicillinase on hollow shells, the lack of antibody binding demonstrates the prevention of antibody access to the enzymes encapsulated within SHELS.

To determine the effect of serum containing neutralizing antibodies on the encapsulated enzyme within SHELS in Figure 6A we compared the activity of the free penicillinase and penicillinase encapsulated within SHELS on nitrocefin ($50 \mu\text{g}/\text{mL}$) in the presence of serial dilutions of serum obtained from immunized mice with penicillinase (see Supporting Information for immunization protocol). The activity of each group was adjusted to $2.5 \text{ IU}/\text{ml}$ in preimmunization serum, and the neutralization is reported as the ratio of the activity in serums

post- to preimmunization. There were around 4×10^9 particles in the SHELS set, making around 4.5 μg of silica. Free penicillinase activity decayed rapidly after dilutions of less than 1:10 000, with activity reduced to less than 5% for all dilutions less than 1:1000. However, even in neat immunized serum, the activity of SHELS was greater than 50%, demonstrating the protection of enzymes against neutralizing antibodies by SHELS encapsulation. The gradual reduction in SHELS activity as serum dilutions decreased may be due to opsonins coating the surface of SHELS, thereby reducing the diffusion of substrate through the nanoporous shell. This result clearly shows the protection of enzymes against neutralizing antibodies by SHELS encapsulation.

To determine whether the protection from neutralization was transient, penicillinase-encapsulated SHELS with 10 IU/ml activity were incubated for 14 days in neat serum obtained from mice immunized with penicillinase. No loss of activity was observed. Moreover, the addition of proteinase-K did not affect the activity level, indicating that encapsulated enzymes were still protected during the experiment (Figure 6B).

To determine whether enzymes encapsulated in SHELS are in a free state within the hollow interior, embedded within the shell, or adsorbed on the interior of the shell, the kinetic parameters⁵⁰ of encapsulated and free *Escherichia coli* L-asparaginase were compared; (see Supporting Information, Figure S7) both free and encapsulated L-asparaginase followed similar Michaelis–Menten kinetics.⁵⁰ The maximum reaction rate achieved by the enzyme–substrate system at the saturating substrate concentration, V_{\max} , was 0.3087 $\mu\text{M}/\text{min}$ for the encapsulated enzyme and 0.3108 $\mu\text{M}/\text{min}$ for free enzyme. The Michaelis constant, K_m , was calculated as 0.001838 mM for encapsulated L-asparaginase and 0.001989 mM for free L-asparaginase. The turnover number, k_{cat} , was derived as 108.8 for the encapsulated enzyme and 109.6 for free enzyme. This similar behavior as verified using multiple constants might indicate that the majority of the encapsulated enzyme is at a free state within the nanoparticle's hollow interior.

To confirm the feasibility of enzymatic therapies with SHELS, protection against neutralization and sustained activity in the presence of serum opsonins and other serum proteins are shown next, in addition to in vivo activity and in-tissue-residence of particles. To demonstrate such activity in vivo, *Gaussia princeps* luciferase encapsulated in SHELS ($\sim 4 \times 10^{12}$ particles/ml) labeled with Cyanine 7 (Cy7) dye were injected subcutaneously into BALB/c mice, followed by lateral tail vein injection of 150 μg native-coelenterazine after 5 min (Figure 6C). Luminescence intensity was measured 5 min after intravenous injection. Luminescence from GaLuc (Figure 6C right panel) was colocalized with the Cy7 fluorescence from SHELS (Figure 6C left panel) proving the in vivo activity of encapsulated GaLuc. Instability of GaLuc at body temperature prevented the detection of in vivo enzymatic activity at later time points (see Supporting Information, Figure S8).

The residence time of SHELS in tissue is important for potential applications such as amino acid depletion therapy. Cy7-labeled SHELS were injected intramuscularly (Figure 6D) and repeatedly imaged over 2 months. A gradual clearance extending to 2 months was observed.

Finally, to illustrate the activity of SHELS in a therapeutically relevant setting, L-asparaginase-loaded SHELS were prepared. For over 40 years, L-asparaginase from *Escherichia coli* has been used to treat acute lymphoblastic leukemia (ALL) in order to deplete circulating L-asparagine, which, unlike normal cells,

cannot be synthesized by leukemic cells. L-asparagine is converted into aspartic acid and ammonia by L-asparaginase's selective starving of leukemic cells, causing cell death.⁴ Immune responses generated against the L-asparaginase are a significant clinical problem and can cause rapid neutralization and clearance of the enzyme as well as significant side effects such as hypersensitivity reactions and anaphylaxis.^{4,8,51} Because an extended residence time in tissue was observed with intramuscular injection previously, this route of administration was chosen for testing the systemic depletion of L-asparagine with either free enzyme or SHELS containing the enzyme. In both cases, the clinically approved enzyme, brand name *Elspar*, was used, and the same total enzyme activity (5 IU) was administered to all mice. The duration of L-asparagine depletion by equivalent amounts of *Elspar* in either naïve (Figure 6E) or passively immunized (Figure 6F) mice was determined. In naïve mice, free enzyme rapidly depleted the serum L-asparagine and kept it at undetectable levels for at least two days. By day five, the serum L-asparagine had recovered completely. *Elspar* given in SHELS (SHELS-*Elspar*) produced a more durable L-asparagine depletion of greater than five days (Figure 6E). When neutralizing anti-L-asparaginase antibodies (verified in Supporting Information, Figure S9) were given before free *Elspar*, L-asparagine depletion was not observed (Figure 6F). However, SHELS-*Elspar* was completely unaffected by the prior introduction of neutralizing antibodies (Figure 6F) verifying the protected operation of enzymes in therapeutically relevant in vivo setting.

Functionalization of SHELS particle surface to improve tissue retention, reduce cell uptake, and protein binding without affecting encapsulated enzyme activity might further prolong the in vivo activity.

Conclusions and Future Potential of SHELS. In summary, SHELS are shown to be a promising platform for encapsulating functional biomolecules, such as enzymes acting on small molecule substrates that can freely diffuse in and out through particles' pores. SHELS can be manufactured in large quantities with sizes and characteristics that can be tightly controlled, thus maximizing entrapment capacity and enzymatic activity. The experimental results show that this porous shell effectively encapsulates the enzyme payload without affecting enzyme activity. The shell also protects the payload from specific and nonspecific interference from large biomolecules in vivo. In addition, surface modifications of SHELS should be able to enhance circulation and targeting in vivo without the need for modification of the payload. As nanomasking provides flexible fabrication of SHELS with control of particle dimensions and permeability, SHELS can be tailored and optimized for specific loads and substrates. Moreover, the utilization of a hollow nanostructure reduces the amount of carrier material introduced into the body. It has also been shown that the SHELS technology prevents the neutralization of nonhuman enzymes by antibodies in vivo and can be used to achieve systemic effects even while these particles remain localized.

The SHELS fabrication approach is general and should be applicable to many other materials. SHELS made of different materials can be envisioned being used in a variety of applications, including nonbiomedical ones such as biocatalysis.

For medical applications, however, toxicity and quantification of the immune response on SHELS will need further study. The effect of surface modifications on the activity of the payload remains to be tested. Indeed, for systemic delivery

applications the surface of SHELS can be further functionalized for targeting and improved circulation half-life, thereby eliminating the need for chemical modification of the enzymic payload. Under these conditions, stealth SHELS should allow continuous and controlled access of the substrate to the native enzyme cargo, which makes this a promising therapeutic platform for treating metastatic disease. In addition, SHELS could be applicable to *in vivo* medical diagnostics and monitoring. Enzyme-prodrug therapy and enzymatic depletion of tumor nutrients are among the most promising applications of SHELS.

■ ASSOCIATED CONTENT

S Supporting Information

Materials, preparations of SHMS, SHELS, SHS, functionalization of SHELS with PEG, labeling of enzymes with Cy5, measurements of activity of penicillinase with CCF2 and nitrocefin, measurements of entrapment capacity, asparaginase activity with Nessler's assay, antibody binding, *in vivo* activity, immunization of mice, Cy7 labeling of SHMS, sustained activity test in immunized serum, testing systemic amino acid depletion and systemic amino acid depletion with passive immunization, characterization, enzyme kinetics calculations, dynamic light scattering data in S1, activity plots of free *Bacillus cereus* penicillinase with and without incubation with proteinase-K in S2, standard curve of *Bacillus cereus* penicillinase in S3, activity plots of different concentrations of free *Bacillus cereus* penicillinase compared to *B. cereus* penicillinase encapsulated within 200 nm SHELS in S4, loading curve of 200 nm SHELS in S5, enzyme activity with respect to loading concentration of 200 nm SHELS in S6, Michealis-Menten plot of ELSPAR encapsulated within SHELS and free ELSPAR in S7, luminescence plots of light reactions of *Gaussia princeps* luciferase with preincubation of different durations, neutralization test in the presence of rabbit polyclonal antibodies against *Elspar* in 1X PBS in S9. This material is available free of charge via the Internet at <http://pubs.acs.org>.

■ AUTHOR INFORMATION

Corresponding Authors

*E-mail: (I.O.) iortac@ucsd.edu.

*E-mail: (S.E.) sesener@ucsd.edu.

Author Contributions

I.O. conceived the idea and designed the study, performed experiments, collected and analyzed data and wrote the paper. D.S., Y.Y., J.Y., B.M., W.C.T., R.Y.T., and S.E. contributed to the study design and preparation of the paper. D.S., Y.Y., and J.Y. contributed to experimental work.

Notes

The authors declare no competing financial interest.

■ ACKNOWLEDGMENTS

The study was supported by the NCI Grant 5U54CA119335-05. We acknowledge the use of the UCSD Cryo-Electron Microscopy Facility, which is supported by NIH grants to T. S. Baker and a gift from the Agouron Institute to UCSD. We acknowledge CallT2 Nano3 Facility for the use of scanning electron microscopes. We are grateful to Kenneth S. Vecchio for the access to scanning transmission electron microscope. We wish to thank I. G. Yayla for his helpful comments and L. Ruff for the help on *in vivo* demonstrations.

■ REFERENCES

- (1) Xu, G.; McLeod, H. L. *Clin. Cancer Res.* **2001**, *7*, 3314–3324.
- (2) Killander, D.; Dohlwitz, A.; Engstedt, L.; Franzén, S.; Gahrton, G.; Gullbring, B.; Holm, G.; Holmgren, A.; Höglund, S.; Killander, A.; Lockner, D.; Mellstedt, H.; Moe, P. J.; Palmbald, J.; Reizenstein, P.; Skärberg, K. O.; Swedberg, B.; Udén, A. M.; Wadman, B.; Wide, L.; Åström, L. *Cancer* **1976**, *37*, 220–228.
- (3) Ni, Y.; Schwaneberg, U.; Sun, Z.-H. *Cancer Lett.* **2008**, *261*, 1–11.
- (4) Ortega, J. A.; Nesbit, M. E.; Donaldson, M. H.; Hittle, R. E.; Weiner, J.; Karon, M.; Hammond, D. *Cancer Res.* **1977**, *37*, 535–540.
- (5) Hu, J.; Cheung, N.-K. V. *Int. J. Cancer* **2009**, *124*, 1700–1706.
- (6) Rooseboom, M.; Commandeur, J. N. M.; Vermeulen, N. P. E. *Pharmacological Reviews* **2004**, *56*, 53–102.
- (7) Bagshawe, K. D. In *Prodrugs*; Stella, V. J., Borchardt, R. T., Hageman, M. J., Oliyai, R., Maag, H., Tilley, J. W., Eds.; Springer New York: New York, 2011; Vol. V, pp 525–540.
- (8) Cheung, N. K.; Chau, I. Y.; Coccia, P. F. *Am. J. Pediatr. Hematol./Oncol.* **1986**, *8*, 99–104.
- (9) Armstrong, J. K.; Hempel, G.; Koling, S.; Chan, L. S.; Fisher, T.; Meiselman, H. J.; Garratty, G. *Cancer* **2007**, *110*, 103–111.
- (10) Zeidan, A.; Wang, E. S.; Wetzler, M. *Expert Opin. Biol. Ther.* **2009**, *9*, 111–119.
- (11) Ascierto, P. A.; Scala, S.; Castello, G.; Daponte, A.; Simeone, E.; Ottaiano, A.; Beneduce, G.; Rosa, V. D.; Izzo, F.; Melucci, M. T.; Ensor, C. M.; Prestayko, A. W.; Holtzberg, F. W.; Bomalaski, J. S.; Clark, M. A.; Savaraj, N.; Feun, L. G.; Logan, T. F. *J. Clin. Oncol.* **2005**, *23*, 7660–7668.
- (12) Kim, J.; Grate, J. W.; Wang, P. *Trends Biotechnol.* **2008**, *26*, 639–646.
- (13) Kim, J.; Grate, J. W. *Nano Lett.* **2003**, *3*, 1219–1222.
- (14) Veronese, F. M. *Biomaterials* **2001**, *22*, 405–417.
- (15) Slowing, I. I.; Vivero-Escoto, J. L.; Wu, C.-W.; Lin, V. S.-Y. *Adv. Drug Delivery Rev.* **2008**, *60*, 1278–1288.
- (16) Xu, Z. P.; Zeng, Q. H.; Lu, G. Q.; Yu, A. B. *Chem. Eng. Sci.* **2006**, *61*, 1027–1040.
- (17) Piras, A. M.; Chiellini, F.; Fiumi, C.; Bartoli, C.; Chiellini, E.; Fiorentino, B.; Farina, C. *Int. J. Pharm.* **2008**, *357*, 260–271.
- (18) Reddy, M. K.; Labhasetwar, V. *FASEB J.* **2009**, *23*, 1384–1395.
- (19) Dziubla, T. D.; Karim, A.; Muzykantov, V. R. *J. Controlled Release* **2005**, *102*, 427–439.
- (20) Cellesi, F.; Tirelli, N. Enzyme Nanoencapsulation in silica gel based nanoparticles. Towards development of novel nanocarriers for enzyme-mediated therapies. <https://www.escholar.manchester.ac.uk/uk-ac-man-scw:2d1981> (accessed Nov 29, 2012).
- (21) Wang, Y.; Caruso, F. *Chem. Commun.* **2004**, 1528–1529.
- (22) Volodkin, D. V.; Petrov, A. I.; Prevot, M.; Sukhorukov, G. B. *Langmuir* **2004**, *20*, 3398–3406.
- (23) Kumar, R.; Maitra, A. N.; Patanjali, P. K.; Sharma, P. *Biomaterials* **2005**, *26*, 6743–6753.
- (24) Wang, Y.; Caruso, F. *Chem. Mater.* **2005**, *17*, 953–961.
- (25) Napierska, D.; Thomassen, L. C. J.; Lison, D.; Martens, J. A.; Hoet, P. H. *Part Fibre Toxicol.* **2010**, *7*, 39.
- (26) Caruso, F.; Shi, X.; Caruso, R. A.; Susha, A. *Adv. Mater.* **2001**, *13*, 740–744.
- (27) Macdonald, J. E.; Bar Sadan, M.; Houben, L.; Popov, I.; Banin, U. *Nat. Mater.* **2010**, *9*, 810–815.
- (28) Arnal, P. M.; Comotti, M.; Schüth, F. *Angew. Chem.* **2006**, *118*, 8404–8407.
- (29) Skrabalak, S. E.; Au, L.; Li, X.; Xia, Y. *Nat. Protocols* **2007**, *2*, 2182–2190.
- (30) Hyuk, Im. S.; Jeong, U.; Xia, Y. *Nat. Mater.* **2005**, *4*, 671–675.
- (31) Blanco, A.; Chomski, E.; Grabczak, S.; Ibisate, M.; John, S.; Leonard, S. W.; Lopez, C.; Meseguer, F.; Miguez, H.; Mondia, J. P.; Ozin, G. A.; Toader, O.; van Driel, H. M. *Nature* **2000**, *405*, 437–440.
- (32) Cochran, J. K. *Curr. Opin. Solid State Mater. Sci.* **1998**, *3*, 474–479.
- (33) Dinsmore, A. D.; Hsu, M. F.; Nikolaides, M. G.; Marquez, M.; Bausch, A. R.; Weitz, D. A. *Science* **2002**, *298*, 1006–1009.

- (34) Kim, S.-W.; Kim, M.; Lee, W. Y.; Hyeon, T. *J. Am. Chem. Soc.* **2002**, *124*, 7642–7643.
- (35) Zhao, M.; Zheng, L.; Bai, X.; Li, N.; Yu, L. *Colloids Surf, A* **2009**, *346*, 229–236.
- (36) Ma, Y.; Qi, L. *J. Colloid Interface Sci.* **2009**, *335*, 1–10.
- (37) Yang, J.; Lind, J. U.; Troglar, W. C. *Chem. Mater.* **2008**, *20*, 2875–2877.
- (38) Guo, X.; Deng, Y.; Tu, B.; Zhao, D. *Langmuir* **2009**, *26*, 702–708.
- (39) Tasciotti, E.; Liu, X.; Bhavane, R.; Plant, K.; Leonard, A. D.; Price, B. K.; Cheng, M. M.-C.; Decuzzi, P.; Tour, J. M.; Robertson, F.; Ferrari, M. *Nat. Nanotechnol.* **2008**, *3*, 151–157.
- (40) Torney, F.; Trewyn, B. G.; Lin, V. S.-Y.; Wang, K. *Nat. Nanotechnol.* **2007**, *2*, 295–300.
- (41) Popplewell, J. F.; King, S. J.; Day, J. P.; Ackrill, P.; Fifield, L. K.; Cresswell, R. G.; di Tada, M. L.; Liu, K. *J. Inorg. Biochem.* **1998**, *69*, 177–180.
- (42) Radin, S.; El-Bassyouni, G.; Vresilovic, E. J.; Schepers, E.; Ducheyne, P. *Biomaterials* **2005**, *26*, 1043–1052.
- (43) Ow, H.; Larson, D. R.; Srivastava, M.; Baird, B. A.; Webb, W. W.; Wiesner, U. *Nano Lett.* **2005**, *5*, 113–117.
- (44) Sokolov, I.; Naik, S. *Small* **2008**, *4*, 934–939.
- (45) Zhu, Y.; Shi, J.; Shen, W.; Dong, X.; Feng, J.; Ruan, M.; Li, Y. *Angew. Chem., Int. Ed.* **2005**, *44*, 5083–5087.
- (46) Bush, K.; Jacoby, G. A. *Antimicrob. Agents Chemother.* **2010**, *54*, 969–976.
- (47) Vrudhula, V. M.; Svensson, H. P.; Senter, P. D. *J. Med. Chem.* **1995**, *38*, 1380–1385.
- (48) Zlokarnik, G.; Negulescu, P. A.; Knapp, T. E.; Mere, L.; Burres, N.; Feng, L.; Whitney, M.; Roemer, K.; Tsien, R. Y. *Science* **1998**, *279*, 84–88.
- (49) Gao, W.; Xing, B.; Tsien, R.; Rao, J. *J. Am. Chem. Soc.* **2003**, *125*, 11146–11147.
- (50) Chen, W. W.; Niepel, M.; Sorger, P. K. *Genes Dev.* **2010**, *24*, 1861–1875.
- (51) Killander, D.; Dohlwitz, A.; Engstedt, L.; Franzén, S.; Gahrton, G.; Gullbring, B.; Holm, G.; Holmgren, A.; Höglund, S.; Killander, A.; Lockner, D.; Mellstedt, H.; Moe, P. J.; Palmblad, J.; Reizenstein, P.; Skärberg, K. O.; Swedberg, B.; Udén, A. M.; Wadman, B.; Wide, L.; Ahström, L. *Cancer* **1976**, *37*, 220–228.